Experimental Study of Multi-Bubble Dynamics Below a Small Anode Using an Air-Water Model

Ali Amiri-Gheisvandi[1], Simon Laliberté-Riverin[2], Ryan M. Soncini[3], Patrice Doiron[4], Gelareh Momen[5], Houshang Darvishi-Alamdari[6] and Seyed Mohammad Taghavi[7]

1. PhD student
7. Full Professor
Department of Chemical Engineering, Université Laval, Québec, Canada
2. Postdoctoral Fellow
6. Full Professor
Department of Mining, Metallurgical and Materials Engineering, Université Laval, Québec, Canada
3. Senior Modelling Engineer
Alcoa – Operational Excellence Center of Excellence, New Kensington, USA
4. Global Manager Modelling and Pilot Operations
Alcoa – Operational Excellence Center of Excellence, Deschambault, Canada
5. Full Professor
Department of Applied Sciences, Université du Québec à Chicoutimi (UQAC), Québec, Canada
1, 2, 6, 7. Aluminum Research Center-Regal, Université Laval, Québec, Canada
Corresponding author: seyed-mohammad.taghavi@gch.ulaval.ca
https://doi.org/10.71659/icsoba2024-al041

Abstract

This research investigates several characteristics of multi-bubble motion under the bottom surface of a reduced-scale carbon anode sample in a physical air-water model of the Hall-Héroult cell. Applying the principles of similarity to our experimental setup, we used low-temperature water and air to represent the bath and CO_2 molecules in the real cell. Ultra-speed camera imaging and videography technique was implemented to track the bubble evolution under the anode from initial generation to detachment from the anode bottom surface. After post-processing the laboratory data using ImageJ, GIMP, and MATLAB, we determined interesting information on the bubble size, residence time, and velocity under the anode. Considering the effect of anode tilt in the longitudinal direction, we demonstrated that increasing the anode tilt reduced the bubble size, residence time, collision, and coalescence under the anode, while bubble velocity was enhanced. Moreover, the threshold initial volume for bubbles to detach from the anode bottom surface at nucleation sites was decreased by increasing the anode tilt. On top of this, the similarity between the bubble size and velocity data that we have determined in our setup and those reported in existing literature, confirms the success of the current configuration in the prediction of the two-phase bubbly layer features beneath the anode. Consequently, we can provide valuable insights for aluminum smelters by optimizing the bubbly layer resistance of our model cell through modification of the geometrical features.

Keywords: Multi-bubble dynamics, Air-water model of the Hall-Héroult cell, Tilted anode, Bubble size, Bubble collision and coalescence.

1. Introduction

In the high-temperature aluminum reduction cell, a reaction between the carbon in the anode and dissolved alumina during the Hall-Héroult process produces CO_2 bubbles beneath the anode. Bubble behavior is illustrated in Figure 1. Small bubbles begin to form under the anode, grow, and eventually merge into larger ones. As they move towards the anode edges, bubbles will detach from the bottom of the anode. The released bubble has the ability to induce circulation in the

surrounding liquid (Figure 1(d)). This complex phenomenon plays a significant role in magnetohydrodynamic (MHD) instability and current efficiency [1]. However, due to the harsh operating conditions and high temperatures within the aluminum reduction cells, studying bubble behavior below the anode surface in the aluminum cell is challenging.

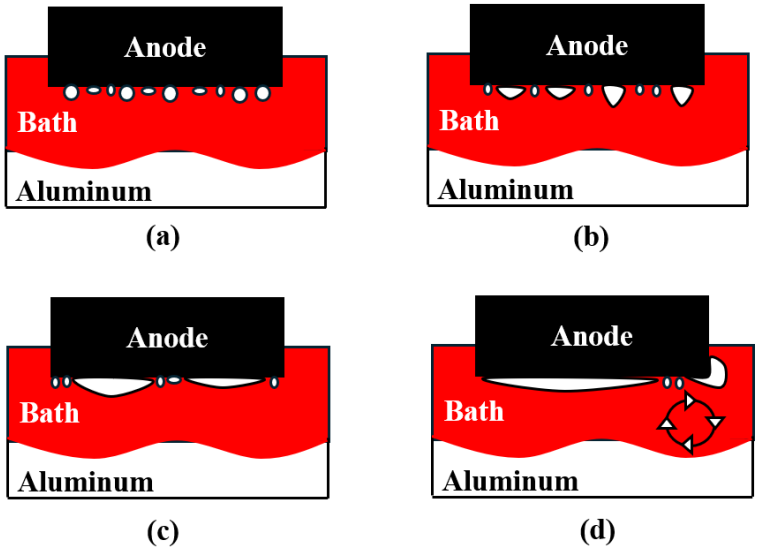

Figure 1. Schematic representing the motion of bubbles under the anode bottom surface: (a) microbubble nucleation, (b) bubble coalescence, (c) bubble swallowing, and (d) bubble detachment.

In recent years, several studies have been conducted on various aspects of bubble transient motion under the anode in the Hall-Héroult process. In an experimental study, Maneri and Zuber [2] conducted the first investigation on the formation of gas bubbles under a tilted anode. Vekony et al. [3] used a full-sized air-water electrolysis cell model to examine the formation of the bubbly layer under the anode. They reported that the larger bubbles tend to absorb the smaller and slower ones, with a maximum height of 2 cm. Additionally, they found that gas bubbles under the anode increases the ohmic resistance of the cell, resulting in higher energy consumption. Alam et al. [4] utilized a one-fourth size aqueous $CuSO_4$ model of the Hall-Héroult cell to study bubble behavior under a flat anode. Their findings indicated that as the anode tilt increased from 0° to 3°, the thickness and size of the bubble layer decreased, along with reduced bubble coverage under the anode. Aaberg et al. [5] measured gas production under the anode by monitoring liquid levels during the electrolysis process. They observed that the bubble thickness ranged from 0.4 cm to 0.6 cm, occasionally reaching 0.71 cm before release from the anode edge. Fortin et al. [6] used a full-scale air-water model of a 150 kA prebaked anode sample to study the morphology of the bubbly layer under the anode. They found that the coverage factor of the bubbles under the anode is influenced by the anode tilt angle, ranging from 24 % to 90 %. Further research by various authors [5, 7-9] supports the idea that the bubble coverage value can vary from 30 % to 90 %, resulting in an additional voltage drop in the cell. Haupin [10] inserted a probe-type reference electrode between the anode and cathode to directly measure the voltage drop of the industrial cell, noting a minimum bubbly layer thickness of 0.5 cm. Das et al. [11] observed that bubble size decreases as the anode tilt increases, while Shekhar and Evans [12] found that a tilted anode leads to a narrower bubble layer beneath the anode. The thickness of the bubble layer estimated to be around 0.4 cm by Xue and Oye [13].

Apart from the mentioned features, many studies have investigated other aspects of bubble motion under the anode, such as bubble velocity and volume. Perron et al. [14] conducted a

comprehensive set of theoretical and experimental investigations to study the behavior of small bubbles moving under an inclined surface. They examined bubble volumes ranging from 0.3 cm^3 to 9 cm^3 and various inclination angles, from horizontal to 10 degrees. Their findings revealed that bubbles with larger volumes and steeper angles have higher terminal velocities. Perron and Kiss [14, 15] studied the motion of individual bubbles under an inclined surface in an air-water model, showing that the terminal velocity of bubbles increases with the surface inclination angle. Masliyah et al. [16]. investigated the velocity of very fine air bubbles moving on an inclined surface in water-glycerin solutions, reporting bubble volumes ranging from 0.0026 cm^3 to 0.013 cm^3. Their results indicated that the terminal velocity of bubbles increased steadily as the tilt angle approached the vertical state. Maxworthy [17] researched the motion of large bubbles in an air-water gravity-driven system beneath an inclined plate, with bubble volumes ranging from 5 cm^3 to 60 cm^3. The study found that the terminal velocity of bubbles increases with their volumes and reaches a maximum of 50 cm/s at approximately 50 degrees of anode tilt. Chen et al. [18] conducted experiments to investigate the effects of bubble volume and surface slope on the terminal velocity of bubbles, contrary to the findings of Maxworthy, Perron and Kiss [14, 15], [17], claiming that the terminal velocity decreases steadily with the anode tilt angle.

In this study, considering the literature gaps, we used a novel low-temperature air-water physical laboratory model of a real Hall-Héroult cell to investigate bubble movement under a pre-baked reduced-scale carbon anode sample. We measure bubble dynamics characteristics such as size, thickness, volume, and velocity after post-processing the laboratory data. Additionally, we analyze the effects of anode tilt angle on these characteristics of bubble motion under the anode. In the following sections, we will describe the methodological approach of this research, present the results, and discuss their implications. Finally, we will conclude our study.

2. Methodological Approach

In this research, we have constructed a novel laboratory-scale air-water model of a real aluminum reduction cell that is safe, affordable, and environmentally friendly. Our aim is to study the behavior of bubbles beneath a carbon anode sample using this physical laboratory model.

Our primary objective in building the low-temperature air-water model was to maintain geometric, kinematic, and dynamic similarities between the real Hall-Héroult cell and the laboratory model. We constructed a one-fifth-scale physical model of the Hall-Héroult cell while maintaining complete geometric similarity. Additionally, we considered five dimensionless numbers: Froude number (Fr), Reynolds number (Re), Weber number (We), Bond number (Bo), and Morton number (Mo), as detailed by Alam et al. [4], in order to maintain both kinematic and dynamic similarities.

The schematic of our experimental setup is depicted in Figure 2. This model includes a rectangular carbon anode sample measuring 32×12×5 cm^3 positioned inside a transparent box. (The slab was extracted from a vertical slice of a green anode manufactured at Alcoa Deschambault. Then it was placed in an Inconel 625 box and was covered with coke particles to prevent air burning. Baking was done in a laboratory furnace (IFS 363635, Pyradia, Canada) up to a temperature of 1100 °C, which was maintained for a soaking time of 20 h [19]). Plastic supports are utilized to maintain the anode and adjust the anode tilt. LED lamps and opaque sheets are used to achieve uniform light distribution under the anode. The camera (Canon EOS R5 with a Canon RF 24-70 mm lens) allows for tracking bubble motion under the anode from both bottom and front views.

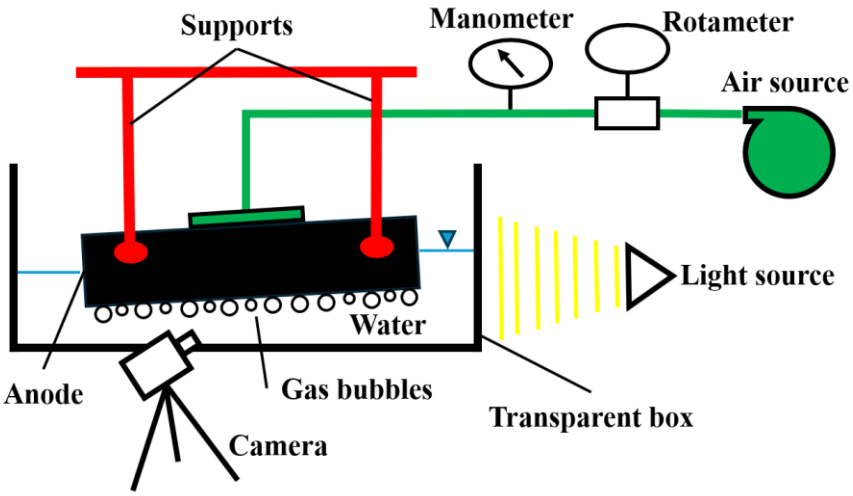

Figure 2. The schematic of the experimental setup.

The transparent box is initially filled with water at room temperature to begin the experiment. Once the initial configuration (Figure 3) is set up, a high-pressure air flow is introduced into the system. A rotameter and a manometer are employed in the flow path to precisely adjust the air pressure and flow rate before compressing the air into the anode pores. Subsequently, uniform bubble generation starts under the anode, and bubbles travel under the anode bottom surface towards the nearest edges. The process of monitoring bubble motion under the anode begins by positioning the camera and activating the light source. Various characteristics of bubble motion under the anode, such as bubble size, velocity, residence time (the time it takes for a bubble to travel between generation sites and release edges is referred to as bubble residence time), collision, and coalescence, are examined under the effect of anode tilt.

Table 1 displays the range of key parameters used in this study.

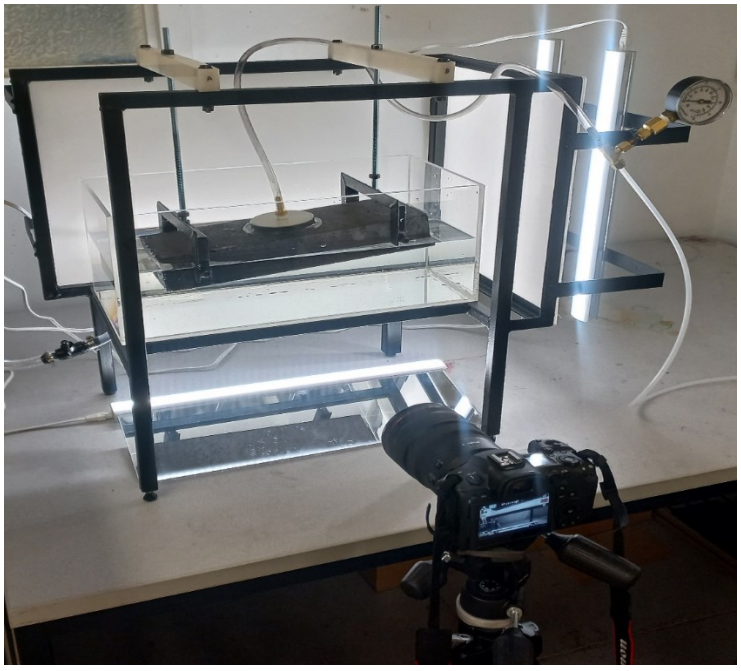

Figure 3. Experimental setup.

Table 1. The range of key parameters.

Key Parameter	Anode Tilt (°)	Air Pressure (kPa)	Air Flow Rate (L/s)	Temperature (K)
Range	0, 1	140	0.0878	298.15

We utilized GIMP, ImageJ, MATLAB, and digital camera to analyze the features of bubble movement beneath the anode. After recording the bubble motion at a specific frame rate (120 /s), we used GIMP and ImageJ software to correct and adjust the reference grid on the captured images (Figure 4 illustrates an example of a corrected image). The thickness of the bubbly layer under the anode was measured using pixel information in ImageJ. The velocity of bubbles beneath the anode was calculated by analyzing the output images from GIMP and ImageJ using PIVlab software in MATLAB. Additionally, we determined the diameter of the bubbles under the anode through light intensity and edge detection methods in MATLAB. Finally, we employed the following formulas [4] to calculate the bubble coverage ratio and bubble volume per unit surface area under the anode bottom surface:

$$\emptyset = \frac{\sum_{j=1}^{n}(\frac{\pi \times {d_j}^2}{4})}{A} \quad (1)$$

$$V = \emptyset \times h \quad (2)$$

where:

$\emptyset$ Bubble coverage ratio, %

d_j the diameter of the j^{th} bubble, mm

n Total number of bubbles, -

A Anode bottom area, mm^2

V Bubble volume per unit surface area, mm^3/mm^2

h Bubble thickness, mm.

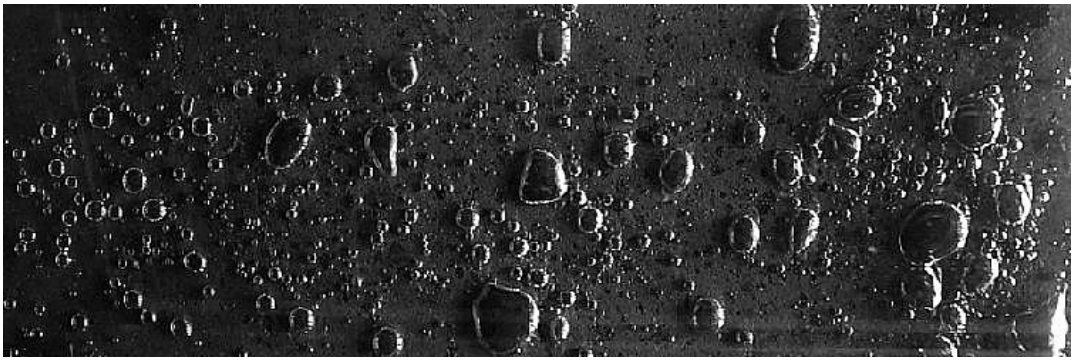

Figure 4. Corrected image using GIMP and ImageJ software.

3. Results and Discussion

The bubbles produced under the anode seen from the front view are depicted in Figure 5. Figure *5*(a) and Figure *5*(b) show the bubbly layer at anode tilts of 0° and 1°, respectively. As seen in these figures, the mean bubbly layer thickness decreases with increasing anode tilt, confirming the findings of Alam and Das [4, 12]. Table 2 demonstrates that the thickness reduction by increasing the anode tilt from 0° to 1° is equal to 15 %. The main reason for this phenomenon is the positive effect of buoyancy, which improves bubble detachment from the nucleation sites, preventing the bubbles from becoming thicker due to insufficient time. The data reported for bubble residence time in Table 2 confirms the observation regarding the bubble thickness. A 29 % decrease in bubble residence time is observed with increasing anode tilt from 0° to 1°. In this

study, bubble residence time was calculated using the FPS characteristic of the high-speed camera in each frame of bubble observation.

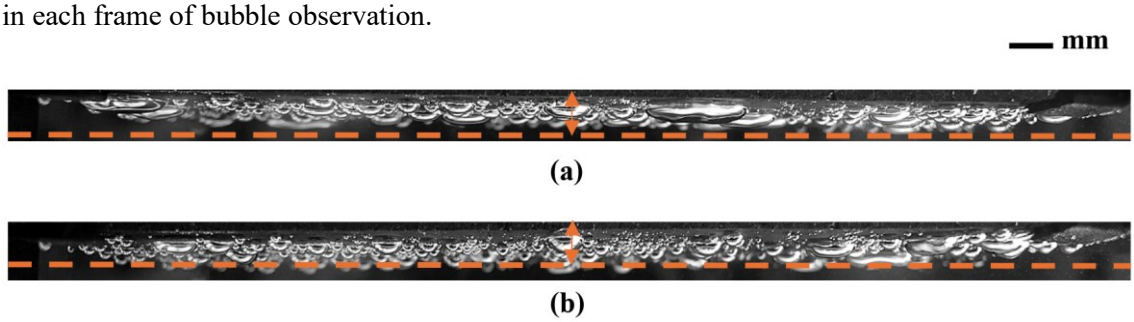

Figure 5. Front view of the bubble morphology at different anode tilts: (a) 0° and (b) 1° (dash lines and arrows indicate the bubbly layer thickness in each figure).

Table 2. The calculated mean values for bubble motion features.

Tilt Angle, (°)	Bubbly Layer Thickness, (mm)	Bubble Diameter Before Release, (mm)	Bubble Volume Per Unit Surface Area, (mm^3/mm^2)	Bubble Residence Time, (s)	Bubble Coverage Ratio, (%)	Global Mean Velocity, (m/s)
0°	1.41	3.56	0.44	1.7417	29	0.0022
1°	1.26	3.01	0.25	1.2424	15	0.0146

Figure 6 shows the bubbles produced under the anode from the bottom view. Again, Figure 6(a) and Figure 6(b) represent the bubbles at different anode tilts of 0° and 1°, respectively. The bubble size decreases with increasing anode tilt, confirming the results of Alam and Das [4, 11]. Table 2 reports a 15 % decrease in bubble diameter before release with increasing anode tilt. As previously mentioned, the main reason for this process is again the buoyancy force. Bubbles detach from the nearest edges of the anode for the horizontal case (Figure 5(a)); however, for the tilted anode, bubbles move along the tilt angle and mostly detach from the furthest edges (surface A-A in Figure 6(b)).

It was also observed that increasing the anode tilt led to an increase in the frequency of bubble collision and coalescence. Micro-bubbles generated at nucleation sites merged into larger bubbles at the region before release sites (surface A-A (down stream)) after collision and coalescence with each other. This confirms the findings of Poncsak [20]: Small bubbles concentrated under the inner edge, while the outer edge had a few large bubbles.

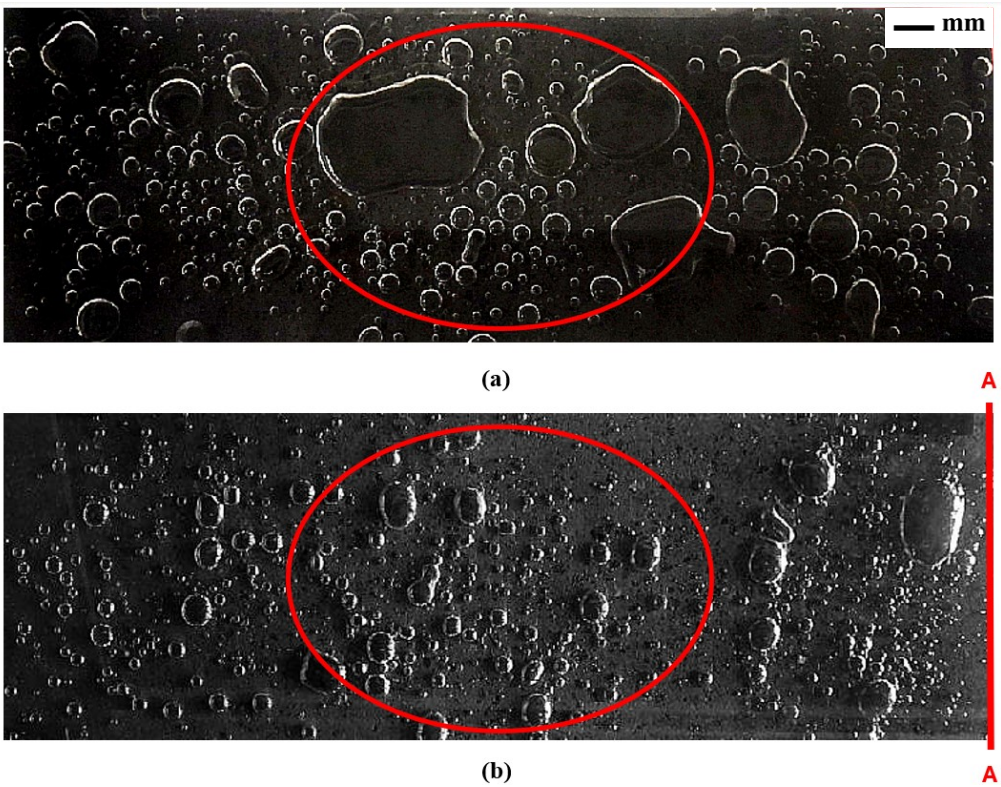

Figure 6. Bottom view of the bubble morphology at different anode tilts: (a) 0° and (b) 1°.

Figure 7(a) and Figure 7(b) show the bubble mean diameter distribution at tilt angles of 0° and 1°, respectively. These diagrams, drawn after analyzing the bottom view of bubble production, demonstrate the probbility of the existence of a bubble with a certain diameter under the anode. Upon comparison between Figure 7(a) and Figure 7(b), it is evident that the probability density of bubbles with large diameters decreases with increasing tilt angle. Moreover, distribution curves (based on Kernel Epanechinkov distribution, Equation (3)) for the bubble diameter (red graphs) in Figure 7(a) and Figure 7(b) show two points (P1 and P2) referring to the most common bubble diameters under the anode for the two cases.

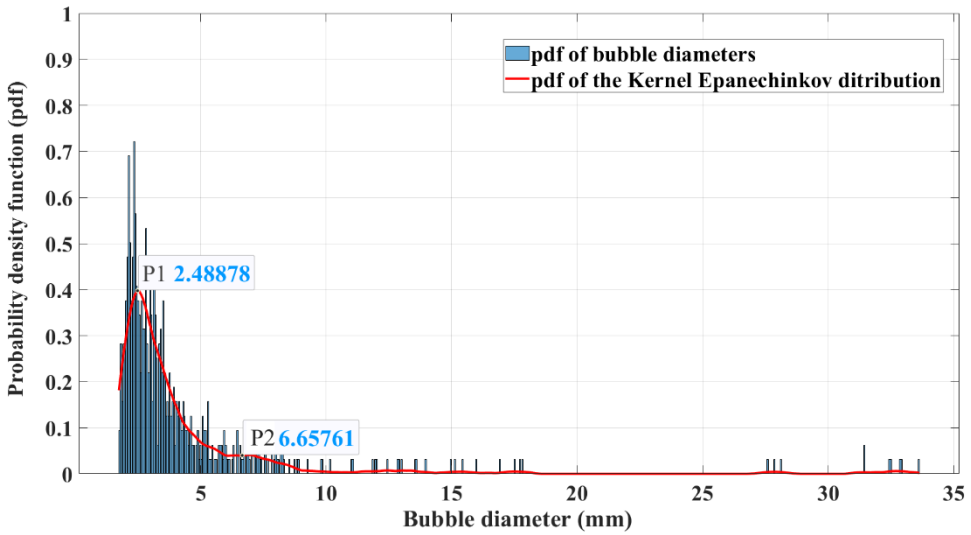

(a)

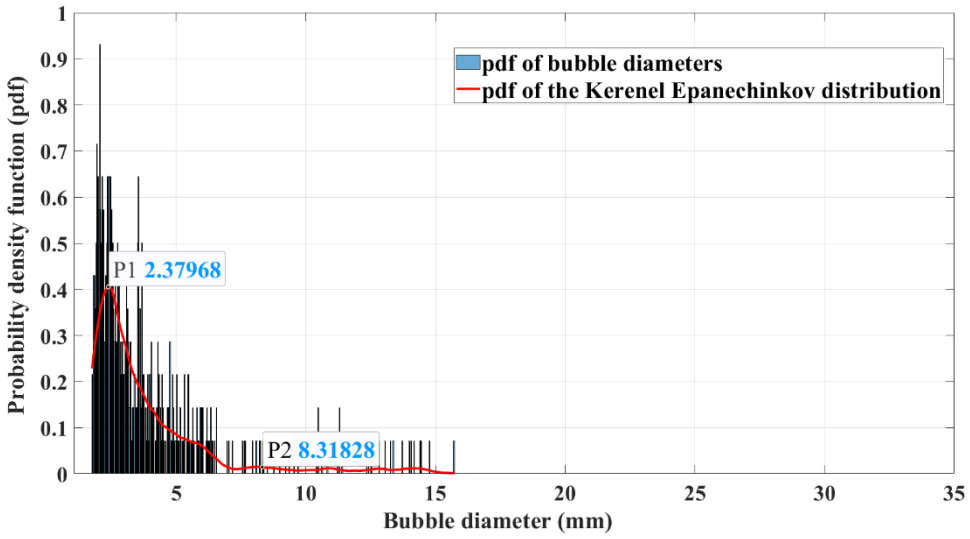

(b)

Figure 7. Bubble diameter frequency at different anode tilts: a) 0° and b) 1°.

Analyzing the distribution curve reveals that P1 remains constant across the two cases, referring to bubbles with 2.4 mm in diameter, while the second common bubble diameter (P2) changes from 6.6 mm to 8.3 mm with a lower probability densisty by increasing the anode tilt from 0° to 1°.

$$\hat{f}(D;h) = \frac{1}{n}\sum_{i=1}^{n} K(z)\left(\frac{D-D_i}{h}\right) \qquad ; K(z) = \frac{3}{4}(1-z^2)1_{\{|z|<1\}} \tag{3}$$

where:

$\hat{f}(D;h)$ Kernel density estimator
$K(z)$ Epanechinkov Kernel
h Band width
n Total number of bubbles
D Bubble diameter
D_i The diameter of ith bubble

After analyzing the bottom view of the bubbles generated and measuring their diameters, we can use Equation 1 and Equation 2 to calculate the bubble coverage ratio and the bubble volume under the anode, respectively. The calculated values are represented in Table 2. It is evident from this table that the bubble coverage ratio and mean bubble volume decrease significantly with an increase in the anode tilt, confirming the results of Alam and Fortin [4, 6]. The main reason for the decrease in the bubble coverage ratio and the mean bubble volume is that the mean bubble diameter decreases with an increase in the tilt angle. Another reason for the decrease in the mean bubble volume is that bubbles start detaching from the generation sites at lower volumes. In Figure 6(a) and Figure 6(b), the red circles indicate the bubble nucleation sites for anode tilts of 0° and 1°, respectively. From these figures, it is evident that the red circle in Figure 6(b) contains smaller bubbles compared to its counterpart in Figure 6(a). Consequently, the initial volume of bubbles to detach from the solid surface at the nucleation site decreases with an increase in the tilt angle.

The bubble mean velocity field under the anode surface is illustrated in Figure 8. Figure 8(a) and Figure 8(b) display the velocity fields at anode tilts of 0° and 1°, respectively. It is clear from these figures that the velocity magnitude increases significantly with an increase in the tilt angle,

confirming the findings of Perron, Kiss, and Maxworthy [3, 14, 17]. For the horizontal anode (Figure 8(a)), there is no regular pattern for the velocity magnitude as the bubbles are released from different edges of the anode. However, for the tilted anode (Figure 8(b)), the bubble velocity field is minimal near the generation sites and reaches its maximum near the release site (surface A-A). The global mean value for bubble velocity (temporal and spatial) is calculated for both anode tilts in Table 2.

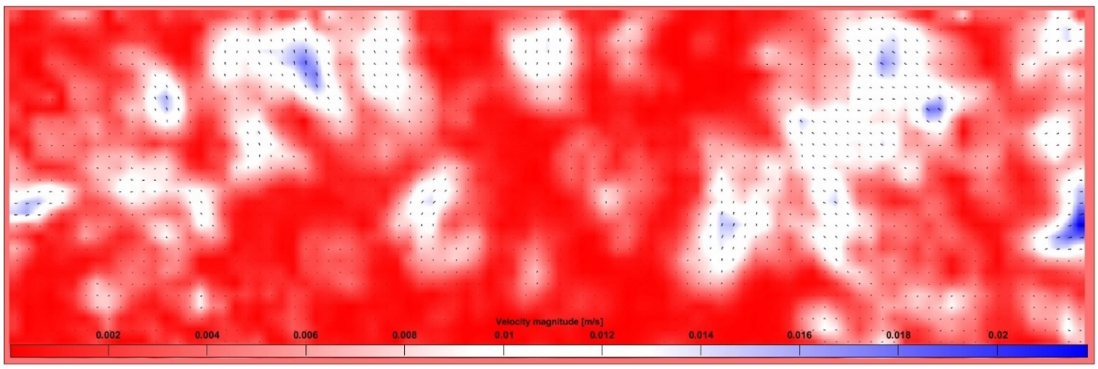

(a)

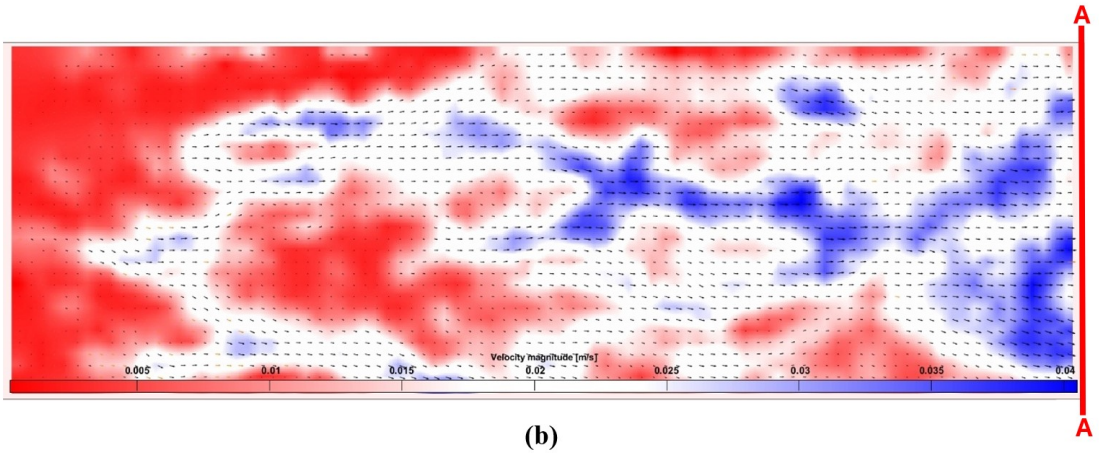

(b)

Figure 8. Bubble velocity field at different anode tilts: a) 0° and b) 1°.

4. Conclusions

In this research, we used a low-temperature air-water laboratory model of the real Hall-Héroult cell to investigate bubble motion under a small-scale pre-baked carbon anode sample. We determined bubble dynamics features such as bubble size, bubble thickness, and bubble coverage under the anode, as well as other characteristics like bubble velocity and bubble volume. The effects of anode tilt angle on these features were also investigated. We used high-speed camera imaging for data measurement and processed the laboratory data using image processing software like ImageJ and MATLAB. The results showed that increasing the tilt angle caused reductions in bubble size, thickness, volume, and coverage under the anode. Conversely, increasing the anode tilt enhanced bubble velocity under the anode surface. It was also observed that the required initial volume for bubbles to start detachment at nucleation sites decreased with an increasing tilt angle. We attribute these results to the positive effects of buoyancy force on bubble motion, which increases with an increasing anode tilt. As previously discussed in this context, there is a good agreement between the results produced by this experimental setup and the current data in the literature. Therefore, we can use this setup and approach to calculate bubbly layer resistance under the anode and find the best feasible tilt angle to minimize this resistance in our laboratory model.

This, in turn, could provide valuable insights to aluminum producers seeking novel geometries to decrease power consumption in industrial cells.

5. Acknowledgement

A part of the research presented in this paper was financed by the Fonds de recherche du Québec - Nature et technologies by the intermediary of the Aluminium Research Centre – REGAL. Additionally, we would like to extend our sincere thanks to Université Laval, the Natural Sciences and Engineering Research Council of Canada (NSERC), and the ALCOA corporation for their support and invaluable collaboration for this research.

6. References

1. Meijia Sun, Baokuan Li, and Linmin Li, Multiscale Simulation of Bubble Behavior in Aluminum Reduction Cell Using a Combined Discrete-Bubble-Model-Volume-of-Fluid-Magnetohydrodynamical Method, *Industrial and Engineering Chemistry Research*, Vol. 58, No. 8 (2019), 3407–3419.
2. C. C. Maneri and N. Zuber, An experimental study of plane bubbles rising at inclination, International Journal of Multiphase Flow, Vol. 1, No. 5 (1974), 623–645.
3. Klára Vékony and László I. Kiss, Morphology of two-phase layers with large bubbles, *Metallurgical and Materials Transactions B*, Vol. 41 (2010), 1006–1017.
4. Morshed Alam, William Yang, Krishna Mohanarangam, Geoffrey Brooks, and Yosry S. Morsi, Investigation of Anodic Gas Film Behavior in Hall–Héroult Cell Using Low Temperature Electrolyte, *Metallurgical and Materials Transactions B*, Vol. 44, No. 5 (2013), 1155–1165.
5. R. J. Aaberg, V. Ranum, K. Williamson, and B. J. Welch, The Gas Under Anodes in Smelting Cells. Part II: Gas Volume and Bubble Layer Characteristics, *Light Metals* 1997, 341-346.
6. S. Fortin, M. Gerhardt, and A. J. Gesing, Physical modeling of bubble behavior and gas release from aluminum reduction cell anodes, *Light Metals* 1984, 721–741.
7. Kaiyu Zhang, Yuqing Feng, Phil Schwarz, Zhaowen Wang, and Mark Cooksey, Computational fluid dynamics (CFD) modeling of bubble dynamics in the aluminum smelting process, *Industrial & Engineering Chemistry Research*, Vol. 52, No. 33 (2013), 1378–11390.
8. W. D. Zhang, J. J. J. Chen, and M. P. Taylor, Similarity Analysis of Gas Induced Bath Flow in Hall-Héroult Cells, in Chemeca 90: *The Eighteenth Australasian Chemical Engineering Conference; Processing Pacific Resources*, Chemical Engineering Group (New Zealand) Auckland, NZ, 1990, 1–8.
9. Ernest W. Dewing, The chemistry of the alumina reduction cell, *Canadian Metallurgical Quarterly*, Vol. 13, No. 4 (1974), 607–618.
10. Warren E Haupin, A scanning reference electrode for voltage contours in aluminum smelting cells, *JOM*, Vol. 23, No. 10 (1971), 46–49.
11. Sbrat Das, Yos S. Morsi, Geoffrey Brooks, John J. J. Chen, and William Yang, Principal characteristics of a bubble formation on a horizontal downward facing surface, *Colloids Surf A Physicochem Engineering Aspects*, Vol. 411 (2012), 94–104.
12. R. Shekhar and J. W. Evans, Physical modeling studies of electrolyte flow due to gas evolution and some aspects of bubble behavior in advanced hall cells: Part I. Flow in cells with a flat anode, *Metallurgical and Materials Transactions B*, Vol. 25 (1994), 333–340.
13. Jilai Xue and Harald A. Oye, Bubble behavior- cell voltage oscillation during aluminum electrolysis and the effects of sound and ultrasound, *Light Metals* 1995, 265–271.
14. A. Perron, L. I. Kiss, and S. Poncsák, An experimental investigation of the motion of single bubbles under a slightly inclined surface, *International Journal of Multiphase Flow*, Vol. 32, No. 5 (2006), 606–622.

15. A. L. Perron, L. I. Kiss, and S. Poncsák, Motion of singles bubbles moving under a slightly inclined surface through stationary liquids, *International Journal of Multiphase Flow*, Vol. 32, No. 12 (2006), 1311–1325.
16. J. Masliyah, R. Jauhari, and M. Gray, Drag coefficients for air bubbles rising along an inclined surface, *Chemical Engineering Science*, Vol. 49, No. 12 (1994), 1905–1911.
17. T. Maxworthy, Bubble rise under an inclined plate, *J Fluid Mech*, Vol. 229 (1991), 659–674.
18. J. J. J. Chen, Jian Chao Zhao, and Kang Xiang Qian, Rise velocity of air bubble under a slightly inclined plane submerged in water, *International Conference on Fluid Machinery*, 1992, 1173–1176.
19. Asem Hussein, Doinald Picard, Houshang Alamdari, Biopitch as a binder for carbon anodes: Impact on carbon anode properties, *ACS Sustainable Chemistry & Engineering*, Vol. 9, No. 12 (2021), 4681–4687.
20. Laszlo I. Kiss, Sandor Poncsak, and Jacques Antille, *Light Metals* 2005, 559–564.